The Astrophysical Journal, 833:223 (8pp), 2016 December 20 doi:10.3847/1538-4357/833/2/223


# DETERMINING PITCH-ANGLE DIFFUSION COEFFICIENTS FROM TEST PARTICLE SIMULATIONS

Alex Ivascenko[1], Sebastian Lange[2], Felix Spanier[1], and Rami Vainio[3]
[1] Centre for Space Research, North-West University, 2531 Potchefstroom, South Africa; alex.ivascenko@rub.de
[2] Lehrstuhl für Astronomie, Universität Würzburg, Emil-Fischer Str. 31, D-97074 Würzburg, Germany
[3] Department of Physics and Astronomy, University of Turku, Finland
*Received 2016 August 22; revised 2016 October 4; accepted 2016 October 10; published 2016 December 19*

## ABSTRACT

The transport and acceleration of charged particles in turbulent media are topics of great interest in space physics and interstellar astrophysics. These processes are dominated by the scattering of particles off magnetic irregularities. The scattering process itself is usually described by small-angle scattering, with the pitch-angle coefficient $D_{\mu\mu}$ playing a major role. Since the diffusion coefficient $D_{\mu\mu}$ can be determined analytically only for the approximation of quasilinear theory, the determination of this coefficient from numerical simulations has become more important. So far these simulations have yielded particle tracks for small-scale scattering, which can then be interpreted using the running diffusion coefficients. This method has a limited range of validity. This paper presents two new methods that allow for the calculation of the pitch-angle diffusion coefficient from numerical simulations. These methods no longer analyze particle trajectories and instead examine the change of particle distribution functions. It is shown that these methods provide better resolved results and allow for the analysis of strong turbulence. The application of these methods to Monte Carlo simulations of particle scattering and hybrid MHD-particle simulations is presented. Both analysis methods are able to recover the diffusion coefficients used as input for the Monte Carlo simulations and provide better results in MHD simulations, especially for stronger turbulence.

*Key words:* diffusion – magnetohydrodynamics (MHD) – methods: numerical – scattering – turbulence

## 1. INTRODUCTION

It is a well-established fact that the transport of energetic charged particles in the heliosphere and the interstellar medium is a convection process along magnetic fields and a diffusive process governed by the collisionless interaction of the particles with magnetic irregularities. A basic concept to describe diffusive particle transport is the Fokker–Planck equation. One of the most important Fokker–Planck coefficients for small-angle scattering is the pitch-angle diffusion coefficient $D_{\mu\mu}$. The importance of this parameter lies in its connection to observable quantities and the mean free path of a charged particle in plasma. The common analytical approaches to deriving $D_{\mu\mu}$ use strong approximations, primarily the quasilinear theory (QLT), first suggested by Jokipii (1966). The fundamental approximation of the QLT is the assumption of *unperturbed orbits*—that is, charged particles follow their gyro-trajectories without any disturbance. This is only valid in weakly turbulent plasma. As the $\delta B/B_0$ ratio and hence the turbulence strength increase, particles are scattered significantly, and the QLT cannot be applied.

To overcome the problems with analytic approaches, numerical simulations have been undertaken. A common approach there is to assume an artificial turbulence spectrum in which tracks of charged particles are followed and the parallel and perpendicular diffusion coefficients are calculated (Michalek & Ostrowski 1997; Qin et al. 2002). Since spatial diffusion coefficients can be derived from pitch-angle diffusion coefficients and satellite observations yield pitch-angle distribution functions, it is more interesting to use test particle simulations to derive the pitch-angle diffusion coefficient directly (Wisniewski et al. 2012).

For a number of reasons, the derivation of the pitch-angle diffusion coefficient is far more complicated than the derivation of spatial diffusion coefficients. One of the main reasons is the changing pitch angle when one traces particle tracks in real turbulence, which leads to a failure of the classical method of running diffusion coefficients since the pitch-angle diffusion coefficient has to be calculated per pitch angle. This has also been shown by Qin & Shalchi (2009), who conclude that due to the rapidly changing $\mu$ in strong turbulence, the pitch-angle diffusion coefficient cannot be determined with the running diffusion method. Despite the limitations of the method, it has nevertheless been successfully used to derive pitch-angle diffusion coefficients from numerical simulations and gain insights into the nature of diffusive particle transport, e.g., scattering at $\mu = 0$ (Qin & Shalchi 2014) and subdiffusion in 2D turbulence (Qin & Shalchi 2009).

In this paper, we present new approaches to calculating $D_{\mu\mu}$ and compare them to the QLT derivations. These methods are distinguished from common derivations of $D_{\mu\mu}$ by their applicability independent of the $\delta B/B_0$ ratio.

## 2. THEORY

### 2.1. Particle Transport Basics

Particle transport in turbulent media is a stochastic process, which is typically described using a statistical approach. An extensive discussion of the foundations can be found in Schlickeiser (2002). For our study the derivation of the transport theory from the Vlasov equation is not especially important. We will focus on the Fokker–Planck equation, which can be derived from the QLT, first suggested by Jokipii (1966) in the context of energetic charged particle transport in turbulent magnetic fields. The fundamental assumption is that of unperturbed particle orbits. This implies the fluctuation amplitudes are small, leading to a quasilinear system. The Vlasov equation for the particle distribution function $F_T$ then

simplifies to (Schlickeiser 2002)

$$\frac{\partial F_T}{\partial t} + v\mu\frac{\partial F_T}{\partial Z} - \Omega\frac{\partial F_T}{\partial \phi} = S_T(X_\sigma, t) + \frac{1}{p^2}\frac{\partial}{\partial X_\sigma}\left(p^2\frac{\partial F_T}{\partial X_\eta}\underbrace{\int_0^t ds\,\langle g_{X_\sigma} g_{X_\eta}(X_\eta, s)\rangle}_{D_{X_\sigma X_\eta}}\right). \quad (1)$$

This equation is known as the Fokker–Planck equation, with the Fokker–Planck coefficients $D_{X_\sigma X_\eta}$, where $X_\sigma, X_\eta$ are generalized coordinates. One of the most interesting parameters is the pitch-angle diffusion coefficient $D_{\mu\mu}$. It describes the pitch-angle scattering of the particle and is consequently connected to the scattering mean free path, which can be evaluated by the observable angular distribution and particle transport simulations (Agueda et al. 2009).

When $D_{\mu\mu}$ is the dominant component, one may simplify the Fokker–Planck equation to

$$\frac{\partial F_T}{\partial t} + v\mu\frac{\partial F_T}{\partial Z} - \Omega\frac{\partial F_T}{\partial \phi} = \frac{\partial}{\partial \mu}\left(D_{\mu\mu}\frac{\partial}{\partial \mu}F_T\right). \quad (2)$$

This in turn can be further simplified after averaging over phase angles $\phi$ and space to

$$\frac{\partial F_T}{\partial t} = \frac{\partial}{\partial \mu}\left(D_{\mu\mu}\frac{\partial}{\partial \mu}F_T\right). \quad (3)$$

In this context, scattering represents a resonant wave–particle interaction of the $n$th order which fulfills the condition

$$k_\parallel v_\parallel - \omega + n\,\Omega = 0, \quad n \in \mathbb{Z} \quad (4)$$

(cf. Schlickeiser 1989), where $\omega$ is the wave frequency, $k_\parallel$ is its parallel wave number, $\Omega$ is the gyro-frequency, and $v_\parallel$ is its parallel velocity component. Different components of the waves contribute for certain values of $n$—namely, the Cherenkov resonance with $n = 0$ is generated by either compressible waves or pseudo-Alfvén waves in the incompressible regime through the mirror force induced by magnetic compressions. Shear Alfvén waves with a wave vector strictly parallel to the background magnetic field ($k_\perp = 0$) fulfill the resonance condition in Equation (4) only for $n = \pm 1$, while for $k_\perp \neq 0$, resonances with $|n| > 1$ are possible (as a result of non-vanishing higher-order Bessel functions in the derivation).

### 2.2. Particle Transport: Numerical Approach

We use two different numerical approaches in this paper to simulate particle scattering: the first method is based on a Monte Carlo approach which produces pitch-angle distributions using a prescribed diffusion coefficient, and the second method calculates particle scattering from the interaction of charged particles with a turbulent background.

The reason for this two-fold approach is that the first method may be used to validate the results, since we may compare the results with a given input parameter, while the second method is a typical use case. This use case shows a far more realistic spectrum for turbulence.

#### 2.2.1. Validation Using Monte Carlo Methods

To validate the results of the new diffusion coefficient calculation method, it is applied to the output of a Monte Carlo propagation code with a given pitch-angle diffusion coefficient as input. For a detailed description of the code, see Agueda et al. (2008) and Agueda & Vainio (2013).

For the validation of method MII, it is necessary to use a particle distribution which is not zero anywhere ($f(\mu) \neq 0$), where the derivative is not vanishing ($df/d\mu \neq 0$), and which is invertible in $\mu$ initially. The choice is otherwise arbitrary. The Monte Carlo method is not affected by any choice of the distribution function.

#### 2.2.2. Application to MHD Turbulence

In order to investigate particle transport in turbulent plasma, a numerical approach is chosen. For this purpose, the parallel hybrid code GISMO is developed, which consists of two parts. GISMO solves the incompressible MHD equation using a pseudospectral method and traces the motion of charged test particles, which interact with the electromagnetic fields generated by MHD turbulence in the plasma. A short description is given in Appendix. For a detailed description, we refer the reader to Lange & Spanier (2012).

The basic setup uses an anisotropic turbulence, which is driven continuously by injecting energy into certain wave modes. The magnetic background field in the first simulation setup is approximately $B_0 = 0.174$ G, which yields, assuming a particle density of $10^5\,\mathrm{cm}^{-3}$, an Alfvén speed of $v_A = 1.2 \times 10^8\,\mathrm{cm\,s}^{-1}$. These values resemble conditions in the solar corona at a distance of three solar radii (Vainio et al. 2003). The outer length scale of the simulated system is $L_{\mathrm{scale}} = 3.4 \times 10^8$ cm. Wave numbers are given in terms of the normalized wave number $k' = kL$. Simulations are performed on a $256^3$ grid.

We use different turbulence setups as described in Lange & Spanier (2012) and Lange et al. (2013):

(1) A turbulence simulation with an anisotropic driver at small wave numbers up to a saturated turbulent stage.
(2) The same turbulence with an amplification of the wave mode at $k_\parallel' = 2\pi \cdot 24$ (further called peak simulation) during the driving stage at small amplitudes.
(3) The peak simulation at the decay stage with QLT-compatible amplitudes.
(4) The peak simulation at the maximum driven stage with big amplitudes, where assumptions of QLT are not fulfilled anymore.

Into the turbulent plasma test particles are injected at least $10^6$ particles. The proton speed is set to a value of $1.21 \times 10^{10}\,\mathrm{cm\,s}^{-1}$, which is chosen to fulfill the resonance condition (Equation (4)). Consequently, a resonant value of $\mu$

$$\mu_R = \frac{\omega - n\,\Omega}{k_\parallel v} = \frac{\omega - n\,\Omega}{L_{\mathrm{scale}}^{-1}\,k_\parallel' v} \quad (5)$$

must be within the interval $[-1, 1]$ for the given particle speed $v$ and wave frequency $\omega$.

The pitch-angle distribution does not affect the plasma dynamics as there is no back-reaction of the particles to the plasma induced. The initial distribution in $\mu$ of the test particles is not important for method MI; only a sufficiently high particle number is needed since this method is statistical. However, the

methods of MII depend on the derivative in $\mu$, which means a significant change to the initial distribution. A half-parabola ($f(\mu) = a \cdot (\mu \pm 1)^2 + c$) distribution is therefore chosen to achieve a non-zero and non-constant derivative.

## 3. METHODS TO DERIVE THE PITCH-ANGLE DIFFUSION COEFFICIENT

In Section 2.1 the fundamental description of the diffusion coefficient $D_{\mu\mu}$ is given. The current section focuses on different concepts to derive $D_{\mu\mu}$ from numerical simulations. We start with common QLT approaches and present new methods afterward.

MI is an established method that relies on the analysis of single particle tracks and serves as a benchmark for the new methods MIIa and MIIb. What both new methods have in common is that they use the particle distribution function for the calculation.

### 3.1. MI Running Diffusion Coefficient

A simple approach for calculating the pitch-angle scattering coefficient is the definition

$$D_{\mu\mu} = \lim_{t\to\infty} \frac{(\Delta\mu)^2}{2\,\Delta t} \overset{t\gg t_0}{\approx} \frac{(\Delta\mu)^2}{2\,\Delta t}, \tag{6}$$

where $\Delta t = t - t_0$ is assumed to be large, i.e., the time evolution $t$ has to be sufficient to develop resonant interactions. This approach is motivated by a description of diffusion where a particle changes its pitch angle by scattering in a randomized process. If the scattering is in resonance with a wave mode, $\Delta\mu$ increases significantly. This method predicts a $\delta$-function shape in the limit of infinite time development. However, in finite intervals of $\Delta t$ the resonances are always broadened. Another problem is the dependence on the strength of the scattering process. In the case of high $\delta B/B_0$ ratios and thus high scattering frequencies, the pitch angle at time $t$ is not connected to its initial state anymore, and the scattering coefficient becomes unstructured (Lange et al. 2013).

### 3.2. MIIa Diffusion Equation Fitting Method

A completely different approach is calculation via the diffusion equation. The basic concept is the assumption of a diffusion process where the pitch-angle diffusion is the predominant process (cf. Equation (3)):

$$\frac{\partial f_T}{\partial t} - \frac{\partial}{\partial\mu} D_{\mu\mu} \frac{\partial f_T}{\partial\mu} = 0. \tag{7}$$

This allows us to calculate the diffusion coefficient from the static particle distribution in $\mu$-space at two distinct timestamps by solving the diffusion equation

$$\frac{\partial f_T(\mu,t)}{\partial t} = \left(\frac{d}{d\mu} D_{\mu\mu}(\mu)\right) \cdot \frac{\partial f_T(\mu,t)}{\partial\mu} + D_{\mu\mu}(\mu) \cdot \frac{\partial^2 f_T(\mu,t)}{\partial\mu^2} \tag{8}$$

numerically for $D_{\mu\mu}(\mu)$.

Since the simulations provide us with discrete distributions, the derivatives are discretized accordingly in the usual way, yielding an equation for every $\mu^n = -1 + n \cdot \Delta\mu$ (with $D^n_{\mu\mu} = D_{\mu\mu}(\mu^n)$):

$$\partial_t f = \frac{D^{n+1}_{\mu\mu} - D^{n-1}_{\mu\mu}}{2 \cdot \Delta\mu} \partial_\mu f + D^n_{\mu\mu} \partial_{\mu\mu} f. \tag{9}$$

This corresponds to a matrix equation with a tridiagonal matrix which can be solved with conventional algorithms:

$$\begin{pmatrix} \partial_{\mu\mu} f^0 & \frac{\partial_\mu f^0}{2\Delta\mu} & 0 & 0 \\ -\frac{\partial_\mu f^1}{2\Delta\mu} & \partial_{\mu\mu} f^1 & \ddots & 0 \\ 0 & \ddots & \ddots & \frac{\partial_\mu f^{n-1}}{2\Delta\mu} \\ 0 & 0 & -\frac{\partial_\mu f^n}{2\Delta\mu} & \partial_{\mu\mu} f^n \end{pmatrix} \cdot \begin{pmatrix} D^0_{\mu\mu} \\ D^1_{\mu\mu} \\ \vdots \\ D^n_{\mu\mu} \end{pmatrix} = \begin{pmatrix} \partial_t f^0 \\ \partial_t f^1 \\ \vdots \\ \partial_t f^n \end{pmatrix}. \tag{10}$$

A problem with this method is the imperfect sampling of the phase space with the test particle approach, which results in a rather noisy distribution function and even noisier derivatives. This can be handled by averaging over several simulation runs, applying smoothing algorithms, or fitting the data with analytical functions.

While ensemble averaging is the correct way to increase the signal-to-noise ratio, it would mean a huge computational effort to obtain more simulation data and cannot be applied at all to real measurements. We find that fitting subsets of the distribution function with low-degree polynomials as described by Savitzky & Golay (1964) is the best way to reproduce the main features of the distribution while reducing noise to a manageable level. An additional advantage of the Savitzky–Golay method is the ease of obtaining derivatives with it.

### 3.3. MIIb Diffusion Equation Integration Method

An additional way to deal with noisy derivatives is to integrate the diffusion equation numerically over $\mu$:

$$\int_{-1}^{\mu} \frac{\partial f_T(\mu,t)}{\partial t} d\mu = D_{\mu\mu}(\mu) \frac{\partial f_T(\mu,t)}{\partial\mu} = -j_\mu(\mu) \tag{11}$$

thus gaining the effective pitch-angle current $j_\mu$ that yields the diffusion coefficient when divided by $\partial_\mu f_T$. The advantage of this method is that the time derivative of $f_T$ is smoothed by the integration and we only need the first derivative in $\mu$, which can also be approximated by a polynomial if necessary.

## 4. RESULTS

### 4.1. Monte Carlo Verification

We first present a validation of the new methods MIIa and MIIb by applying them to the output of a Monte Carlo propagation model with a preset pitch-angle diffusion coefficient of the form

$$D_{\mu\mu}(\mu) = \frac{\nu_0}{2}\left(\frac{|\mu|}{1+|\mu|} + \epsilon\right)(1-\mu^2).$$

The results in Figure 1 show good agreement in shape and absolute value of the diffusion coefficient calculated from

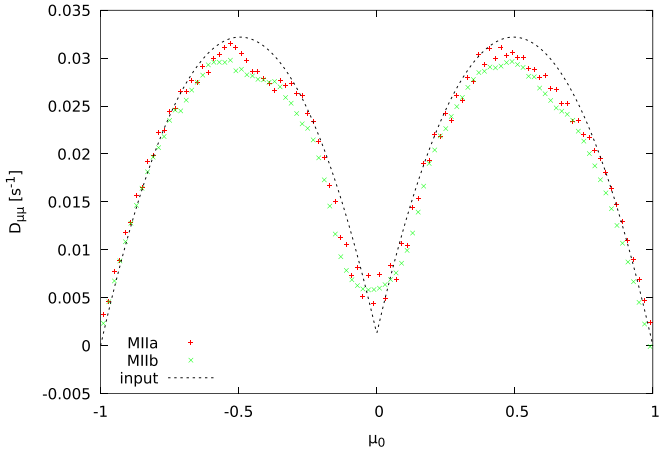


**Figure 1.** Comparison of $D_{\mu\mu}$ used as input for the Monte Carlo propagation model and results obtained from the output with the newly developed methods MIIa and MIIb.

(smoothed) pitch-angle particle distributions as compared to the analytical expression used as input.

### 4.2. Background Simulation Results

For the analysis of MHD simulation results with the new methods, we first apply them to so-called background simulations. These are simulations performed with the GISMO code, where energy is injected into MHD plasma continuously until a steady turbulent spectrum evolves. The Goldreich–Sridhar-like spectrum can be seen in Figure 9. The fluctuation level is rather low ($(\delta B/B_0)^2 \approx 0.001$), which means that the QLT is a relatively good approximation for the transport of charged particles in this case.

In Lange & Spanier (2012) scatter plots were used extensively to display the effect of the diffusion. One such scatter plot is shown in Figure 2. It directly shows the change of the pitch angle $\Delta\mu$ for each particle. This type of plot reveals resonant structures very clearly. Unfortunately, this plot is an appropriate tool only for approaches where the individual particle can be traced.

Figure 3 shows the diffusion coefficient $D_{\mu\mu}$ obtained with the classical running coefficient method MI. The development of a resonant structure is clearly visible as the simulation progresses from 1 to 30 gyration periods. It should be noted that this development is a stochastic effect of an increasing portion of homogeneously distributed particles undergoing resonant interactions with wave modes running through the simulation box and is unrelated to the development of the turbulence itself, which is completed before test particles are injected into the simulation.

The apparent splitting of the maxima at 30 gyrations is caused by the tilt of the resonance peak in $\Delta\mu$ when it is plotted over the initial $\mu_0$, as seen in Figure 2. Calculating $(\Delta\mu)^2$ folds the negative half-peak up, resulting in the apparent double-peak structure. The correct choice of the starting pitch angle $\mu_0$ has been discussed by Tautz et al. (2013). While we agree that this can improve the appearance of the plot, it does not change its fundamental meaning.

The results of the direct integration MIIb in Figure 4 compare very nicely with those of the direct solution of the fitted matrix equation MIIa. Both methods of MII show a maximum at the Cherenkov resonance which is dominating the

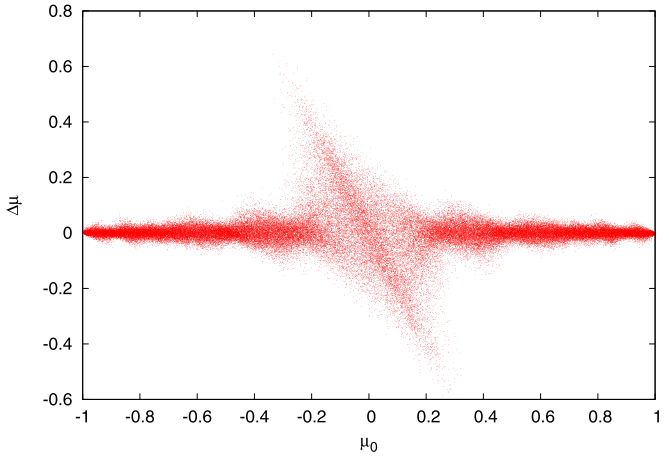


**Figure 2.** Change of the pitch angle $\Delta\mu$ in dependence of the initial value $\mu_0$ for $10^5$ particles within turbulent plasma after 30 gyrations. This *scatter plot* is a valuable tool for investigating resonant interactions. The dominant structure is the Cherenkov resonance $n = 0$.

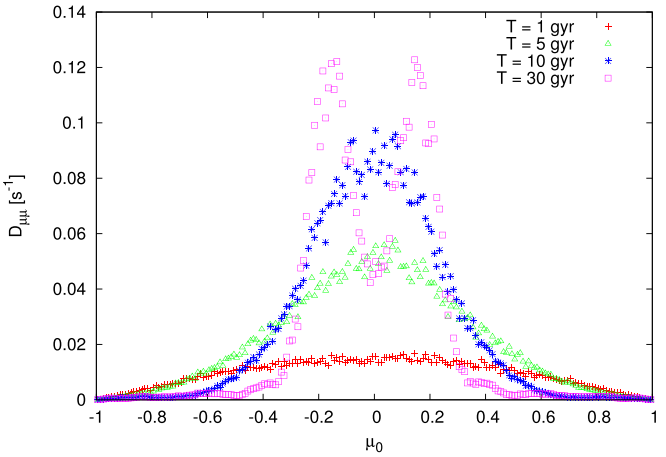


**Figure 3.** Time evolution of the pitch-angle scattering coefficient $D_{\mu\mu}$ calculated by MI. A clear resonant structure develops between 10 and 30 gyration periods. By comparison to the scatter plot in Figure 2 the maxima can be connected to the Cherenkov resonance.

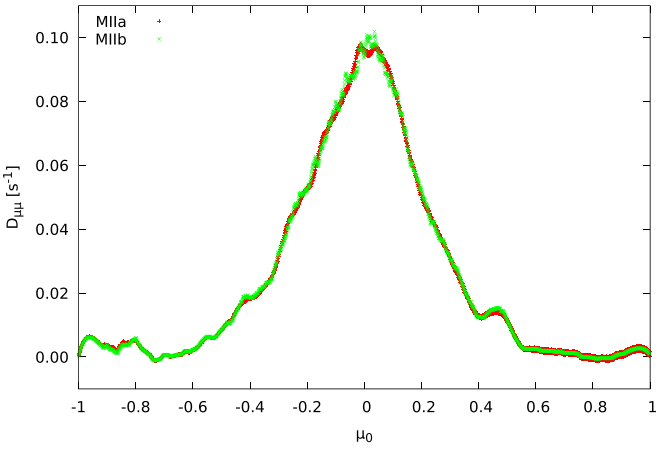


**Figure 4.** Comparison between MIIa and MIIb for the background turbulence simulation clearly showing the Cherenkov resonance. The shown time interval is after 10 gyrations.

scattering (see Figure 2). Unlike that in MI, the maximum does not split due to the tilt shown in the scatter plot. Thus, MII can be used independently and without any interpretative help.

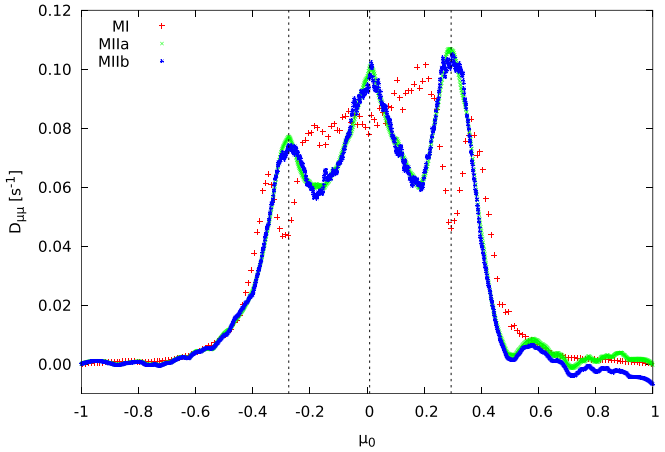


**Figure 5.** Comparison between MI, MIIa, and MIIb for the driven stage of the peak simulation at small amplitudes. The vertical lines indicate the resonance positions according to Equation (4). The shown time interval is after 10 gyrations.

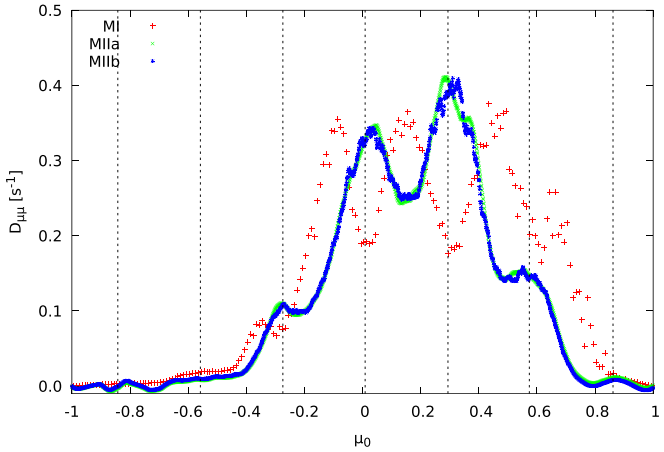


**Figure 6.** Comparison between MI, MIIa, and MIIb for the decay stage of the peak simulation at small amplitudes. The vertical lines indicate the resonance positions according to Equation (4). The shown time interval is after 10 gyrations.

### 4.3. Driven Peak Simulation Results

The next scenario is peak simulation with a driven amplification at $k_{\parallel}' = 2\pi \cdot 24$. In this scenario a background MHD simulation is used, where additional energy is injected at $k'$. This leads to a strong magnetic fluctuation at localized wave modes. This in turn means that the QLT approximation for the particle transport does not hold anymore at those wave modes. This is an interesting test case for the particle transport analysis since QLT may or may not be applicable depending on the time since the onset of peak driving and the particle energy.

First, we present the results at the beginning of the driven stage, where amplitudes are small enough to keep near the quasilinear assumptions. A comparison between MI and MIIa (and MIIb) is presented in Figure 5. The running diffusion coefficient method MI shows again a split of the maxima, so that the predicted resonant positions are right in between. Although this is not correct, it is still interpretable by using the corresponding scatter plot. The methods of MII, however, show again a very nice match to the predicted resonances. The small fluctuations at $\mu = 0.6$, 0.8 and 0.9 are not connected to resonances but indicate the statistical influence of the particle number, which in this simulation is lower at positive pitch angles. All of the three methods show comparable amplitudes in $D_{\mu\mu}$.

### 4.4. Decaying Peak Simulation Results

During the decay stage of the peaked mode, energy spreads due to convection and diffusion toward perpendicular wave numbers. This leads to the increased influence of higher-order resonances and thus a more complex scattering pattern. In Figure 6 we present again a comparison of the results of the different methods during the decay stage of the peak with small amplitudes.

Because the scattering is more complex, we also present the corresponding scatter plot in Figure 7 to interpret the results of MI. The tilt of the resonances causes again the split of the maxima in the results of MI. The left-hand polarization of the wave mode has not developed, and resonances with negative $\mu$ are smaller than $n = 2$ and 3. MIIa and MIIb confirm this.

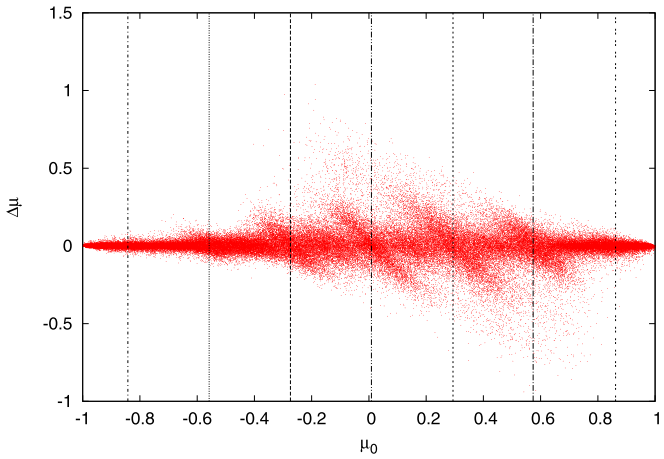


**Figure 7.** Scatter plot of the peak resonance during the decay stage.

### 4.5. Strong Turbulence Results

In order to test the limits of QLT, we present the results of the peak simulation at the maximum driven stage. The local amplitudes reach values of $\delta B/B_0 \approx 1$, where quasilinear assumptions are not valid. Consequently, the results of method MI in Figure 8 are erroneous and also no longer interpretable with the scatter plot. The corresponding scatter plot (not shown here) only shows a broad tilted band where many particles are scattered strongly. Nevertheless, the methods of MII are expectedly not influenced by this. Both results show again the resonant maxima, although there is a larger background scattering.

## 5. CONCLUSION

We have presented two different methods to calculate the Fokker–Planck coefficient $D_{\mu\mu}$. The first method MI depends on the QLT and is thus sensitive to turbulence strength or wave mode amplitudes. Consequently, this method is usable for very small fluctuations ($\delta B$ and $\delta E$) only. Despite this sensitivity to the validity of the QLT assumption, as shown in our results, the method MI is still applicable if the corresponding scatter plots are used for interpretation. Only at big wave amplitudes does this method fail (see Figure 8).

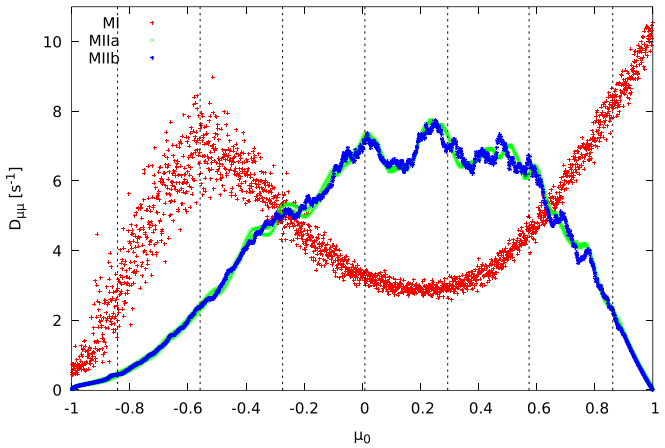


**Figure 8.** Comparison between MI, MIIa, and MIIb for the maximum driven stage of the peak simulation at big amplitudes. The vertical lines indicate the resonance positions according to Equation (4). The shown time interval is after 10 gyrations. The QLT-based MI derives an incorrect $D_{\mu\mu}$, and the match with the resonance at $\mu = -0.56$ is coincidental. Both methods of MII show the maxima at the predicted positions of the resonances.

Both methods of MII are independent of quasilinear assumptions. This is very important for most scenarios. Especially with particle scattering in highly turbulent states or at wave modes with large amplitudes, these methods give correct results. The resonant maxima are not split up, and interpretation with the scatter plots is not necessary, which is another advantage. However, care should be taken considering the assumptions incorporated in the new methods. Since Equation (7) presupposes a purely diffusive process in $\mu$, MII cannot be used directly in the case of anomalous diffusion, in contrast to MI, which can be employed to calculate diffusion coefficients in super- and subdiffusion (Qin & Shalchi 2009). The integer derivatives in Equation (7) change to fractional derivatives in this case, resulting in the equation

$$\frac{\partial f_T}{\partial t} - D_\alpha \mathbb{D}_t^{1-\alpha} \frac{\partial^2 f_T}{\partial \mu^2} = 0 \tag{12}$$

with the fractional derivative defined as

$$\mathbb{D}_t^{1-\alpha} = \frac{1}{\Gamma(\alpha)} \frac{\partial}{\partial t} \int_0^t \frac{f_T(t')}{(t-t')^{1-\alpha}} dt'. \tag{13}$$

While an inversion of this fractional derivative exists mathematically, the actual implementation would involve solving Laplace integrals, making the method even more sensitive to noise and destroying the simple and elegant form of MII.

A different approach could be taken to tackle anomalous diffusion in an approximate manner by calculating $D_{\mu\mu}(t) \propto t^{\alpha-1}$ at successive timesteps with unmodified Equation (7) and determining the fractional order $\alpha$ from it. Unfortunately, to have a chance to see anomalous diffusion in our MHD simulations would require large simulation sizes (for superdiffusion) and long run times (for subdiffusion).

Another assumption of MII concerns the pitch-angle distribution function $f_T(\mu)$. It must have non-zero first and second derivatives in $\mu$ and should change sufficiently between two evaluation timesteps. Consequently, resonances with very small wave amplitudes or those not leading to a change in the $\mu$-distribution are not resolved. In this case, MI should be used.

A.I. and F.S. acknowledge support from NRF through the MWL program. This work is based upon research supported by the National Research Foundation and the Department of Science and Technology. Any opinion, findings, and conclusions or recommendations expressed in this material are those of the authors, and therefore, the NRF and DST do not accept any liability in regard thereto.

## APPENDIX
## DESCRIPTION OF THE GISMO CODE

The GISMO code (Lange & Spanier 2012) was used to determine turbulent fields in incompressible plasma. The set of equations which are solved in the MHD code GISMO are the incompressible MHD equations

$$\frac{\partial \boldsymbol{u}}{\partial t} = \boldsymbol{b} \cdot \nabla \boldsymbol{b} - \boldsymbol{u} \cdot \nabla \boldsymbol{u} - \nabla P + \nu \nabla^{2h} \boldsymbol{u} \tag{14}$$

$$\frac{\partial \boldsymbol{b}}{\partial t} = \boldsymbol{b} \cdot \nabla \boldsymbol{u} - \boldsymbol{u} \cdot \nabla \boldsymbol{b} + \nu \nabla^{2h} \boldsymbol{b} \tag{15}$$

with the magnetic field $\boldsymbol{b} \equiv \boldsymbol{B}/\sqrt{4\pi\rho}$ and constant mass density $\rho$ and fluid velocity $\boldsymbol{u}$. The total pressure is denoted by $P$, which describes both thermal and magnetic pressure, $P = p + B^2/(8\pi)$. Viscous and ohmic dissipation are given by the generalized resistivity $\nu$, which causes wave number diffusion. We also consider here hyperdiffusivity, which occurs for $h > 1$. Especially for fast solar wind, which we are interested in, this fluid can be considered as incompressible. This leads, together with the solenoidality condition for the magnetic field, to the boundary conditions

$$\nabla \cdot \boldsymbol{u} = 0 \tag{16}$$

$$\nabla \cdot \boldsymbol{b} = 0. \tag{17}$$

With these boundary conditions, it is possible to find a closure for the MHD equations. The pressure $P$ may be derived by taking the divergence of the MHD equations. This in turn yields Maron & Goldreich's (2001)

$$\nabla^2 P = \nabla \boldsymbol{b} : \nabla \boldsymbol{b} - \nabla \boldsymbol{u} : \nabla \boldsymbol{u}. \tag{18}$$

The solution for incompressible fluid problems can be achieved by the spectral method.

In the incompressible regime of magnetized plasma, MHD turbulence consists of only two types of waves, which propagate along the parallel direction—the so-called pseudo-Alfvén and shear Alfvén waves. The first type is the incompressible limit of slow magnetosonic waves and plays a minor role within anisotropic turbulence (Maron & Goldreich 2001). The pseudo-Alfvén waves' polarization vector is on the plane spanned by the wavevectors $\boldsymbol{k}$ and $\boldsymbol{B}_0$. Shear waves are transversal modes with a polarization vector perpendicular to the $\boldsymbol{k}$–$\boldsymbol{B}_0$ plane. They are circularly polarized for parallel propagating waves. Both species exhibit the dispersion relation $\omega^2 = (v_A k_\parallel)^2$.

Since the model consists of only these two wave types, it is suitable to use a description with the Alfvénic waves moving either forward or backward. This is achieved by introducing the Elsässer variables (Elsässer 1950),

$$\begin{aligned} \boldsymbol{w}^- &= \boldsymbol{v} + \boldsymbol{b} - v_A \boldsymbol{e}_\parallel \\ \boldsymbol{w}^+ &= \boldsymbol{v} - \boldsymbol{b} + v_A \boldsymbol{e}_\parallel, \end{aligned} \tag{19}$$

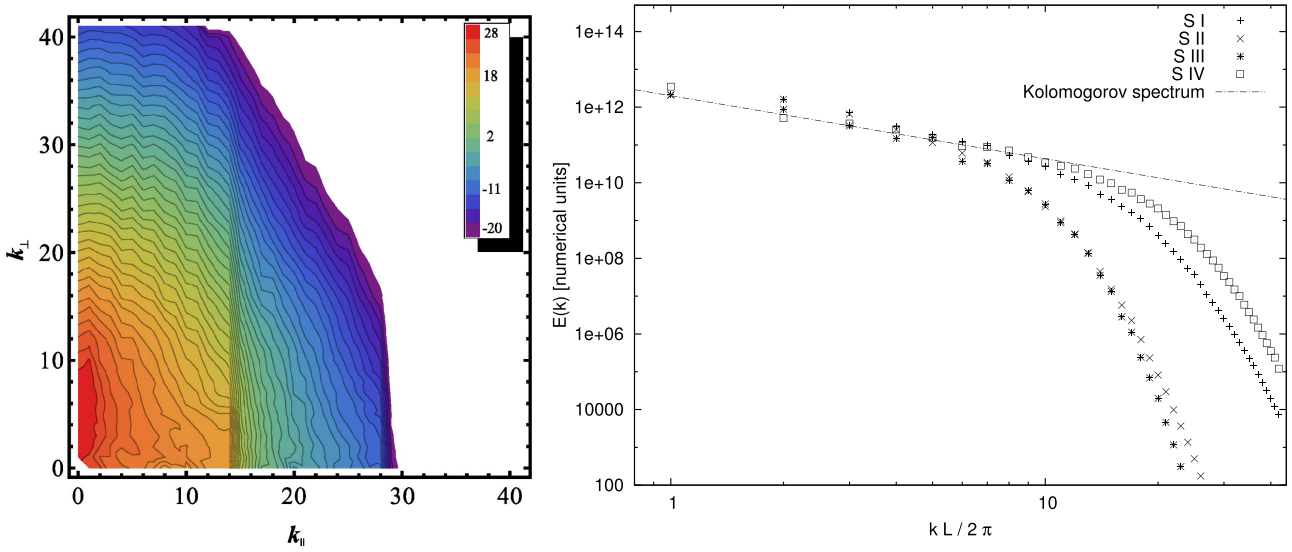


**Figure 9.** Results of the background simulation performed with GISMO. The left figure shows a two-dimensional energy spectrum that clearly shows signs of a Goldreich–Sridhar cascade (Goldreich & Sridhar 1997): energy is transported preferentially along $k_\perp$ until a critical balance is reached, after which energy can also be transported along $k_\parallel$. The figure on the right side shows the corresponding one-dimensional spectrum, which is approximately a $k^{-5/3}$ spectrum.

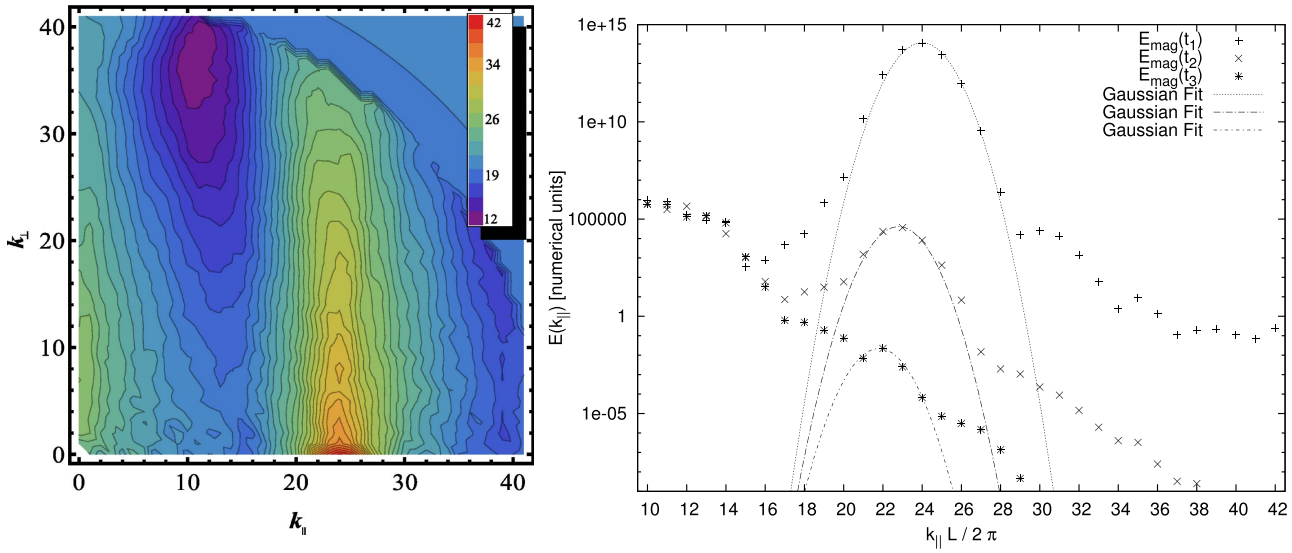


**Figure 10.** Results of a simulation performed with GISMO in which energy is injected at $k = 24$ starting from a background simulation. The left figure shows a two-dimensional energy spectrum, where the transport in the $k_\perp$ direction for the injected energy can also be seen. The figure on the right side shows the corresponding spectrum in the parallel direction, where the added bump from the injected energy can be seen. This is approximately in the dissipation regime of the Kolmogorov spectrum.

and transforming Equations (15) into a suitable form of

$$(\partial_t - v_A k_z)\tilde{w}_\alpha^{\mp} = \frac{i}{2}\frac{k_\alpha k_\beta k_\gamma}{k^2}(\widetilde{w_\beta^{+} w_\gamma^{-}} + \widetilde{w_\beta^{-} w_\gamma^{+}}) - ik_\beta \widetilde{w_\alpha^{\mp} w_\beta^{\pm}} - \frac{\nu}{2}k^{2h}\tilde{w}_\alpha^{\mp}$$
$$k_\alpha \tilde{w}_\alpha^{\pm} = 0. \quad (20)$$

Two important scenarios with regard to the turbulence simulation have been considered:

1. A scenario in which energy is continuously injected at the smallest wave numbers until an equilibrium of driving and dissipation leads to a turbulent inertial range. This is the background simulation (cf. Figure 9) which all other simulations build on. For comparison, the decaying turbulence, when the driving has been turned off, is also studied.
2. Another important scenario is the injection of energy at medium wave numbers, which resembles the energy injected into the plasma by energetic protons (cf. Figure 10). This scenario is interesting in terms of physics since proton beams are one important source of energy, but they are also numerically interesting since the wave number space's local turbulence ratio can reach values of $\delta B/B_0 > 1$.

Into the fields generated by the MHD code, charged test particles are injected. The Lorentz force

$$\frac{d}{dt}\gamma \boldsymbol{v} = \frac{q}{mc}[\, c\boldsymbol{E}(\boldsymbol{x}, t) + \boldsymbol{v} \times \boldsymbol{B}(\boldsymbol{x}, t)], \quad (21)$$

is acting upon the particles. Here the electric field is generated from the MHD fields, assuming an ideal Ohm's law with $\boldsymbol{E} = -\boldsymbol{u} \times \boldsymbol{B} = -1/4(\boldsymbol{w}^- + \boldsymbol{w}^+) \times (\boldsymbol{w}^+ - \boldsymbol{w}^-)$.

A suitable numerical approach for solving Equation (21) for gyrating particles is the implicit scheme of the *Boris push*. The basic idea was given by Boris (1970): the iterations of the Lorentz force are separated into two partial steps. First, the particles are accelerated by the electric field within a half time step. Second, the gyromotion of the particles is calculated, which is caused by the magnetic field. After that, the electric field acts again for another half time step to complete the iteration. This approach leads to a discretization of the Lorentz force (for the detailed set of equations, see Birdsall & Langdon 2005).

The advantage of the Boris push is its very high numerical stability. The particles are assumed to undergo gyromotions; hence, the particle orbits themselves are stable for an arbitrary time discretization. Even in the limit of $\Delta t^{\mathrm{num}} \gg \Omega^{-1}$ the particle orbit is stable, although it converges to an adiabatic drift motion. The limitation of this method is the correct resolution of the Larmor radius $r_{\mathrm{L}}$. If the chosen time step is too large, this would lead to a large deviation from the analytical $r_{\mathrm{L}}$. GISMO–PARTICLES measures the deviation from $r_{\mathrm{L}}$ and adapts it to the preferred value. In our simulations an accuracy of the order of $|r_{\mathrm{L}} - r_{\mathrm{measured}}|/r_{\mathrm{L}} \approx 10^{-5}$ is used.

A limitation to the method of the Boris push is ultra-relativistic particle speeds. In this case the conservation of energy would be violated, since the ideal ohmic law is not fulfilled anymore. Beyond Lorentz factors of $\gamma \approx 10^3$ fictitious forces start to act, and this approach is no longer applicable (Vay 2008).

Both parts of GISMO are calculated for each step. After iterating the Elsässer MHD fields $\boldsymbol{w}^{\pm}$, they are transformed into the physical electric and magnetic fields, which are transferred to GISMO-PARTICLES. Then the Boris push is performed. Each particle responds to its local fields, which are calculated by an averaging method via three-dimensional splines (Spanier & Wisniewski 2011, Wisniewski et al. 2012). Periodic spatial boundary conditions are used; thus, the number of particles remains constant in each simulation.

## REFERENCES


Agueda, N., & Vainio, R. 2013, JSWSC, 3, A10
Agueda, N., Vainio, R., Lario, D., & Sanahuja, B. 2008, ApJ, 675, 1601
Agueda, N., Vainio, R., Lario, D., & Sanahuja, B. 2009, AdSpR, 44, 794
Birdsall, C. K., & Langdon, A. B. 2005, Plasma Physics Via Computer Simulation (1st ed.; New York: Taylor and Francis)
Boris, J. P. 1970, in Proc. Fourth Conf. Numerical Simulation Plasmas (Washington, DC: Naval Research Laboratory), 3
Elsässer, W. M. 1950, PhRv, 79, 183
Goldreich, P., & Sridhar, S. 1997, ApJ, 485, 680
Jokipii, J. R. 1966, ApJ, 146, 480
Lange, S., & Spanier, F. 2012, A&A, 546, A51
Lange, S., Spanier, F., Battarbee, M., Vainio, R., & Laitinen, T. 2013, A&A, 553, A129
Maron, J., & Goldreich, P. 2001, ApJ, 554, 1175
Michalek, G., & Ostrowski, M. 1997, A&A, 326, 793
Qin, G., Matthaeus, W. H., & Bieber, J. W. 2002, ApJL, 578, L117
Qin, G., & Shalchi, A. 2009, ApJ, 707, 61
Qin, G., & Shalchi, A. 2014, PhPl, 21, 042906
Savitzky, A., & Golay, M. J. E. 1964, AnaCh, 36, 1627
Schlickeiser, R. 1989, ApJ, 336, 243
Schlickeiser, R. 2002, Cosmic Ray Astrophysics (Berlin: Springer)
Spanier, F., & Wisniewski, M. 2011, ASTRA, 7, 21
Tautz, R. C., Dosch, A., Effenberger, F., Fichtner, H., & Kopp, A. 2013, A&A, 558, A147
Vainio, R., Laitinen, T., & Fichtner, H. 2003, A&A, 407, 713
Vay, J. 2008, PhPl, 15, 056701
Wisniewski, M., Spanier, F., & Kissmann, R. 2012, ApJ, 750, 150